

Renormalized Lattice Dynamics and Thermal Transport in VO₂

Yi Xia^{1,*} and Maria K. Y. Chan^{1,†}

¹Center for Nanoscale Materials, Argonne National Laboratory, Argonne, IL 60439, USA

(Dated: April 4, 2025)

Vanadium dioxide (VO₂) undergoes a first-order metal-insulator transition (MIT) upon cooling near room temperature. The MIT is concomitant with structural changes from rutile to monoclinic, and an accurate characterization of lattice vibrations is vital for elucidating the underlying phase transition mechanism. To investigate the lattice dynamics and thermal transport properties of VO₂ across the MIT, we present a phonon renormalization scheme based on self-consistent phonon theory through iteratively refining vibrational free energy. Using this technique, we compute temperature-dependent phonon dispersion and lifetime, identify extremely strong anharmonicity associated with low-lying zone-center optical mode, and point out the importance of both magnetic and vibrational entropy in driving the MIT. The predicted phonon dispersion and lifetimes show quantitative agreement with experimental measurements. We demonstrate that lattice thermal conductivity of rutile VO₂ is nearly temperature independent as a result of the strong intrinsic anharmonicity, while that of monoclinic VO₂ varies according to $1/T$. Due to phonon softening and enhanced scattering rates, the lattice thermal conductivity is deduced to be substantially lower in the rutile phase, suggesting that Wiedemann-Franz law might not be strongly violated in rutile VO₂.

Vanadium dioxide (VO₂) is a transition metal oxide under intense study, because it exhibits a first-order metal-insulator transition (MIT) from metallic rutile phase (R-VO₂) to semiconducting monoclinic phase (M-VO₂) upon cooling to near room temperature ($T_{\text{MIT}}=340$ K), which facilitates the realization of near-room-temperature switching of either electronic or thermal conductivity [1]. The mechanism underlying the MIT in VO₂ has been a longstanding subject of controversy due to the coupled changes in structural and electronic properties across the MIT. As a result, various studies have been focused on clarifying whether the MIT is driven by instabilities in electron-lattice dynamics or charge localization due to strong electron-electron correlation [2–6].

In contrast to various existing studies of electronic properties, a comprehensive understanding of lattice dynamics properties has yet to be accomplished, as indicated by limited experimental characterization. From a theoretical point of view, R-VO₂ is challenging due to its strong anharmonicity and lattice metastability. Recent study by Budai *et al.* [7] reveals the important role of vibrational entropy in driving the MIT based on the X-ray/neutron scattering measurements and *ab initio* molecular dynamics (AIMD) calculations. By examining experimentally measured temperature-dependent phonon density of states (DOS), a discontinuity in DOS shape across the MIT is identified, which is associated with the softening of transverse acoustic branches. The change in vibrational entropy was found to be $\Delta S_{\text{ph}}=1.02\pm 0.09 k_{\text{B}}/\text{VO}_2$, which is comparable to the total entropy change of $1.50\pm 0.15 k_{\text{B}}/\text{VO}_2$ from

latent heat measurements [8]. Renormalized phonon dispersions were further computed using temperature-dependent effective potential (TDEP) [9] and AIMD simulations, and found to be consistent with inelastic X-ray scattering (IXS) measurements. The computational and experimental results suggest that phonon dominates over electron to stabilize R-VO₂.

Despite the observed increase by several orders of magnitude in the electrical conductivity, there are only a few studies which address the separate contributions from electron and phonon to thermal transport in VO₂ across the MIT, primarily due to coupled electron and phonon transport in metallic R-VO₂. In a recent study Lee *et al.* [10] attempted to decouple the thermal conductivity of R-VO₂ into two parts, i.e. electron (κ_e) and phonon (κ_l), by explicitly modeling κ_l using experimentally-measured phonon linewidths (and hence lifetimes) and computed phonon dispersions. The resultant value of κ_e in R-VO₂ was anomalously low, implying a significant violation of the Wiedemann-Franz (WF) law, which the authors attributed to unconventional quasiparticle dynamics, i.e. absence of quasiparticles in a strongly correlated electron fluid where heat and charge diffuse independently [10].

Although previous studies found phonon softening to constitute a significant fraction of the total entropy change, the remaining portion is too large to be attributed to electronic entropy (i.e. caused by partial occupancy of electron in Fermi-Dirac statistics). Recent quantum Monte Carlo calculations reveal that both the rutile and monoclinic structures have antiferromagnetic ground states [11]. However, a significant change in magnetic coupling strength across the transition leads to magnetic ordering and disordering in M-VO₂ and R-VO₂ respectively, thus contributing additional entropy to stabilize R-VO₂ [12]. Since κ_e can only be indirectly de-

* yxia@anl.gov

† mchan@anl.gov

terminated by subtracting κ_l from the total thermal conductivity in measurements, accurate modeling of κ_l of R-VO₂ is crucial, therefore calling for a theoretical examination based on first-principles methods. Herein, we first present a phonon renormalization scheme based on extracting temperature-dependent interatomic force constants (IFCs) on top of compressive sensing lattice dynamics (CSLD) [13] through iteratively refining vibrational free energy, and then apply it to perform a comprehensive study of lattice dynamics and thermal transport properties of VO₂. Our study quantitatively clarifies the changes of vibrational entropy and lattice thermal conductivity across the MIT, which reveal the importance of magnetic entropy and suggest that WF law might not be strongly violated in R-VO₂.

Existing methods that are capable of treating strong anharmonic effects nonperturbatively are based on or related to self-consistent phonon theory [14], such as self-consistent *ab initio* lattice dynamics (SCAILD) [15] and stochastic self-consistent harmonic approximation (SSCHA) [16]. The present implementation of phonon renormalization is in the spirit of SCAILD, where vibrational free energy is iteratively refined based on the computed temperature-dependent atomic displacements in each step. As implemented by Roekeghem *et. al.* [17], an improvement over SCAILD can be achieved by using the full quantum mean square thermal displacement matrix, which allows for simultaneous update of both phonon frequencies and eigenvectors. The temperature-dependent atomic displacements $\{u_{a,\alpha}\}$ are generated according to the probability $\rho(\{u_{a,\alpha}\}) \propto \exp(-\frac{1}{2}\mathbf{u}\Sigma^{-1}\mathbf{u})$ to find a displaced configuration in the harmonic approximation, where $u_{a,\alpha}$ is the displacement of atom a in α direction, and Σ is known as the quantum covariance matrix of displacement vector [16, 17]

$$\Sigma_{a\alpha,b\beta} = \frac{\hbar}{2\sqrt{M_a M_b}} \sum_{\lambda} \frac{(1 + 2n_{\omega_{\lambda}})}{\omega_{\lambda}} \epsilon_{a\alpha}^{\lambda} \epsilon_{b\beta}^{*\lambda}, \quad (1)$$

where M , ω , ϵ , n , λ are atomic mass, phonon frequency, eigenvector, Bose-Einstein distribution and branch index respectively. Hence various sets of $\{u_{a,\alpha}\}$ can be generated using the covariance matrix following a given distribution, such as continuous Gaussian distribution or discrete Rademacher distribution, which are used in SSCHA and SCAILD respectively. Note that the current scheme to generate temperature-dependent atomic displacements is superior compared to sampling trajectory from AIMD, which suffers from the absence of the quantum effect of nuclear motion and thus underestimates the thermal displacements for temperatures below Debye temperature (≈ 1000 K for VO₂). A self-consistent loop was formed by generating $\{u_{a,\alpha}\}$ using effective IFCs extracted from previous step. Both 2nd- and 3rd-order IFCs were simultaneously extracted using a recently developed direct method named compressive sensing lattice dynamics (CSLD) [13], in which DFT forces are expressed as a

Taylor expansion in displacements and the coefficients are obtained from sparse regression (see Supplementary Material [18] for more details of CSLD and implementation/validation of our renormalization scheme). From effective harmonic and anharmonic IFCs computed using CSLD, phonon lifetimes were evaluated using Fermi's golden rule by treating 3rd-order IFCs as perturbation to harmonic phonons [19], and linearized Boltzmann transport equation (BTE) was solved in an iterative manner to account for the non-equilibrium phonon distributions [20–23].

Vienna *Ab initio* Simulation Package (VASP) was used to perform structural relaxation and self-consistent calculations [24–27]. The projector-augmented wave (PAW) [28] method was used in conjunction with the generalized gradient approximation (GGA) [29] for the exchange-correlation (xc) functional [30]. Perdew-Burke-Ernzerhof (PBE) and its revised version for solids (PBEsol) [31, 32] xc functionals were used, since recent studies [7, 33] show that (1) PBE tends to predict lattice dynamics properties in good agreement with experiments and (2) PBEsol generally yields better lattice parameter via achieving a more balanced binding energy compared to PBE and LDA. Experimental lattice parameters were found [7], as well as confirmed in this study, to better describe lattice dynamics properties compared to DFT-relaxed structures, therefore structures of experimental lattice parameters with relaxed internal atomic coordinates were used in subsequent calculations. (See Supplemental Material [18] for structural and computational details.)

To confirm the convergence of renormalized phonon dispersions, vibrational free energy of R-VO₂ computed in each iteration, as shown in Fig. 1(a), is examined and found to achieve good convergence to about ± 1 meV/atom after seven iterations. Additional iterations were performed to (1) confirm the convergence and (2) obtain a large pool of forces for eventual IFCs fitting. Without accounting for temperature effect, phonon dispersions of M-VO₂ computed in the harmonic approximation, as shown in Fig. 1(b), have well defined frequencies with positive values, exhibiting normal harmonic behavior. In contrast, there is a large portion of imaginary frequencies (square root of negative eigenvalues of dynamical matrix) in phonon dispersions of R-VO₂ across the Brillouin zone, consistent with previous theoretical studies [7, 10, 34]. With temperature effect considered, the renormalized phonon dispersions of R-VO₂ at 425 K in Fig. 1(c) exhibit hardening of optical modes and achieve overall good agreement with experimental IXS measurements [7], confirming the fact that R-VO₂ indeed can be stabilized by increasing temperature above the MIT. Specifically, the computed high-lying transverse acoustic (TA2), longitudinal acoustic (LA) and low-lying zone-center optical (ZCO) phonon frequencies agree excellently with experiments, while low-lying transverse acoustic (TA1) phonon frequencies display a trend of

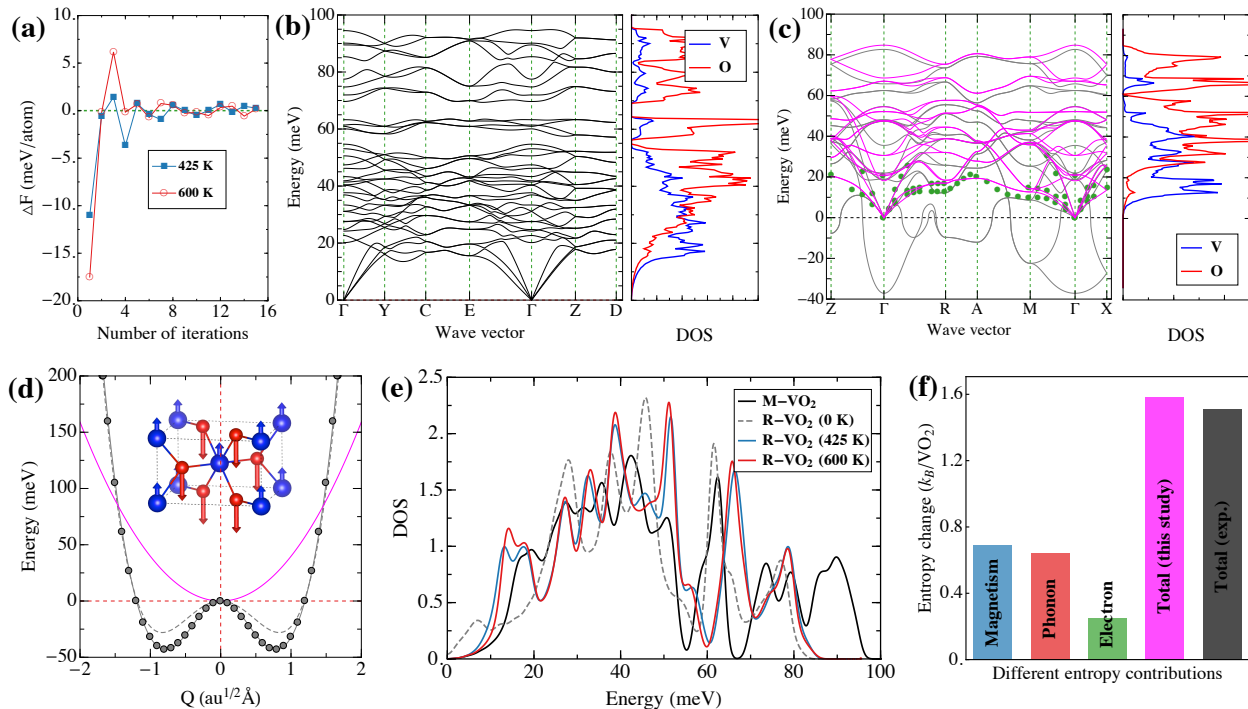


FIG. 1. (a) The change of vibrational free energy between consecutive iterations as a function of the number of iterations in the phonon renormalization process of rutile VO_2 at 425 and 600 K. The green dashed line denotes the converged value of vibrational free energy (set to zero). (b) Computed phonon dispersions and atom-projected density of states (DOS) of monoclinic VO_2 in the harmonic approximation at 0 K. (c) Renormalized phonon dispersions (solid magenta lines) and atom-projected DOS of rutile VO_2 at 425 K in comparison with experimental inelastic X-ray scattering data at 425 K [7] (green disks) and the phonon dispersions computed at 0 K (solid gray lines). Imaginary frequencies are denoted as negative numbers. (d) Potential energy surface of the imaginary phonon mode of rutile VO_2 at Γ point as a function of vibrational amplitude. The solid gray disks denote the computed energies, and dashed/solid gray line denotes polynomial fitting up to 6th/16th order. The solid magenta line represents the effective harmonic potential at 425 K. The inset shows the atomic displacements in accordance with the eigenvector. (e) Total phonon DOS of monoclinic VO_2 at 0 K (solid black lines) and rutile VO_2 at 0 K (dashed gray lines), 425 K (solid blue lines) and 600 K (solid red lines). (f) Separated entropy contributions from magnetic ordering [12], phonons, and electrons [7] across the metal-insulator transition, compared with total entropy change measured from latent heat experiment [8].

overestimation, particularly along Γ -R and Γ -M paths, which probably could be attributed to various approximations utilized in DFT calculations. Renormalized phonon dispersions of R- VO_2 were additionally computed at 360 and 600 K to investigate the temperature dependence. As shown in Fig. S6 [18], the presence of imaginary frequencies in phonon dispersions at 360 K indicates that R- VO_2 tends to be unstable near MIT, and only low-lying ZCO phonon mode is significantly hardened (from 17.8 meV to 23.3 meV) with temperature enhanced from 425 to 600 K, indicating that ZCO phonon mode is severely anharmonic.

To quantitatively investigate the anharmonicity of the ZCO phonon mode, Fig. 1(d) shows its potential energy surface as a function of atomic displacement following the renormalized eigenvector, wherein V and O atoms move away from each other along the rutile c axis. The identi-

fied double-well potential of ZCO phonon mode exhibits structural instability of R- VO_2 , which appears in 0 K phonon dispersions. Indeed, by projecting the renormalized eigenvector onto those zone-center phonon modes computed at 0 K, it is found that ZCO phonon mode matches exactly the zone-center imaginary optical mode. Therefore, the structure of R- VO_2 is a dynamic average over symmetry-broken minima separated by relatively deep energetic barriers (≈ 42 meV), and the positions of V and O atoms represent their averaged spatial occupations, consistent with experimental observations of large thermal displacements [35]. The severe anharmonicity of ZCO mode is also reflected in the detailed shape of its energy profile, which can be fitted using polynomials up to 16th-order, while 6th-order leads to too shallow potential well.

To confirm and explain the experimentally observed

large phonon entropy change across the MIT [7], the total phonon DOS of M- and R-VO₂ are compared in Fig. 1(e). It can be seen that temperature-induced phonon renormalization significantly alters the DOS of R-VO₂. Further increasing temperature from 425 K to 600 K tends to slightly harden low-lying modes while softening high-lying modes. Comparison of total DOS between M- and R-VO₂ displays an abrupt blueshift of low-lying DOS shoulders (≈ 13 meV) with phonon modes notably hardened when temperature is reduced below the MIT. These phonon modes are mainly associated with the TA1 modes near zone boundary and constitute the majority of vibrational entropy change. To quantify it, temperature-dependent vibrational entropy is computed using phonon dispersions of M-VO₂ at 0 K and R-VO₂ at 425 K. As shown in Fig. 1(f), both PBE and PBEsol xc functionals are found to yield very close vibrational entropy change of $0.64 k_B/\text{VO}_2$ at 340 K, which is smaller than $1.02 k_B/\text{VO}_2$ reported by Budai *et al.* [7]. We attribute the discrepancy mainly to the overestimated TA1 modes in our calculation. As a result, total entropy change, which includes contributions of 0.64 and $0.25 k_B/\text{VO}_2$ from lattice vibration and partial occupancy of electrons in R-VO₂ [7] respectively, is smaller than experimental report of $1.50 k_B/\text{VO}_2$ [8]. The additional entropy change might be explained by the magnetic ordering revealed by a recent quantum Monte Carlo simulation [11, 12]. In M-VO₂, singlets are formed due to the strongly coupled magnetic moments within the dimers, which leads to zero entropy for such a state. Whereas above the transition temperature, R-VO₂ is in a magnetic disordered state, contributing roughly $\Delta S = k_B \ln(2) = 0.69 k_B/\text{VO}_2$ to the total entropy change. As shown in Fig. 1(f), the estimated total entropy change accounting for both electron, phonon and magnetism shows a value of $1.58 k_B/\text{VO}_2$, which is in excellent agreement with experimental value of $1.50 k_B/\text{VO}_2$ [8], implying that magnetic ordering is also important in stabilizing the rutile phase.

Having confirmed the present theoretical approach through verifying the computed phonon dispersions and vibrational entropy change against experiments, lattice thermal transport properties were calculated and compared in detail with experiments in Fig. 2. Considering the facts that (1) experiments found that both phonon lifetimes and κ_l of R-VO₂ show no temperature dependence up to 425 K [7, 10] and (2) renormalized phonon dispersions of R-VO₂ at a lower temperature (360 K) shows imaginary modes (see Fig. S6(a) [18]), κ_l of R-VO₂ was computed using renormalized IFCs at 425 K. By comparing the computed κ_l of polycrystalline VO₂ (κ_l averaged over Cartesian coordinates) to experimental measurements on polycrystalline VO₂ reported by Andreev *et al.* [36] and Chen *et al.* [37], as shown in Fig. 2(a), it is found that both theoretical and experimental κ_l of M-VO₂ decrease with increased temperature according to $1/T$, while κ_l of R-VO₂ remains nearly unchanged above

the MIT. κ_l of R-VO₂ at 600 K was further evaluated to investigate its temperature dependence at high temperatures. The PBEsol results show a slightly decreased κ_l from 2.95 to $2.60 \text{ W m}^{-1} \text{ K}^{-1}$ with temperature increased from 425 to 600 K, which is considerably slower than $1/T$ and indicative of the “amorphous” character of heat conduction without presence of significant structural disorder [36]. We find that this weak temperature dependence of κ_l is due to strong anharmonicity, which significantly renormalizes 2nd and 3rd-order IFCs. Compared to experiments, PBE results agree very well with Ref. [36], while both PBE and PBEsol results exhibit overestimation compared to Ref. [37], the later of which is probably caused by the presence of defects such as grain boundaries and pores in R-VO₂ [37]. Nevertheless, both PBE and PBEsol yield significant decrease of κ_l across the MIT (1.4 and $1.0 \text{ W m}^{-1} \text{ K}^{-1}$ for PBE and PBEsol respectively), which is comparable with the value of $1.3 \text{ W m}^{-1} \text{ K}^{-1}$ reported in Ref. [36]. Since κ_l of R-VO₂ in Ref. [36] is evaluated using standard Lorentz number L_0 , the present theoretical results suggest that WF law is not violated in polycrystalline VO₂. However, compared to the estimated κ_l along rutile c axis using first-principles phonon dispersions and phonon scattering rates obtained from the IXS measurements [10] as shown in Fig. 2(b), both PBE and PBEsol results display smaller κ_l for M- and R-VO₂ and a much larger decrease of κ_l across MIT, which is primarily due to the predicted significantly smaller κ_l of R-VO₂. Since κ_l is subtracted from total thermal conductivity to estimate κ_e in Ref. [10], which is subsequently utilized to identify a strong violation of WF law in R-VO₂, it is crucial to confirm and verify κ_l of R-VO₂.

To explore the origin of our predicted lower κ_l of R-VO₂, the full widths at half maximum ($\text{FWHM} = h/\tau$ with lifetime τ) and mean free paths ($\text{MFP} = |\mathbf{v}|\tau$, where \mathbf{v} is group velocity) of phonon modes at 425 K and varying energies are compared with those estimated using IXS measurements [10]. As shown in Fig. 2(c), the predicted FWHMs are consistent with IXS data. Considering the fact that there are many different lifetimes for phonon modes with similar energies and IXS data merely samples a limited space in the full Brillouin zone, to better compare with experiments we computed energy-dependent FWHM weighted by squared phonon group velocity, which is a more rigorous way to average the FWHM than linearly interpolating the phonon modes with small FWHMs as adopted in Ref. [10]. Our predicted energy-dependent FWHM agrees quantitatively with IXS data from low to high phonon energies, further verifying the accuracy of computed phonon scattering rates. The same good agreement is also achieved in mode-resolved MFP, as shown in Fig. 2(d). Our results imply that simple linearly interpolation tends to significantly overestimate/underestimate FWHMs of phonon modes with low/high energies, in addition to neglecting

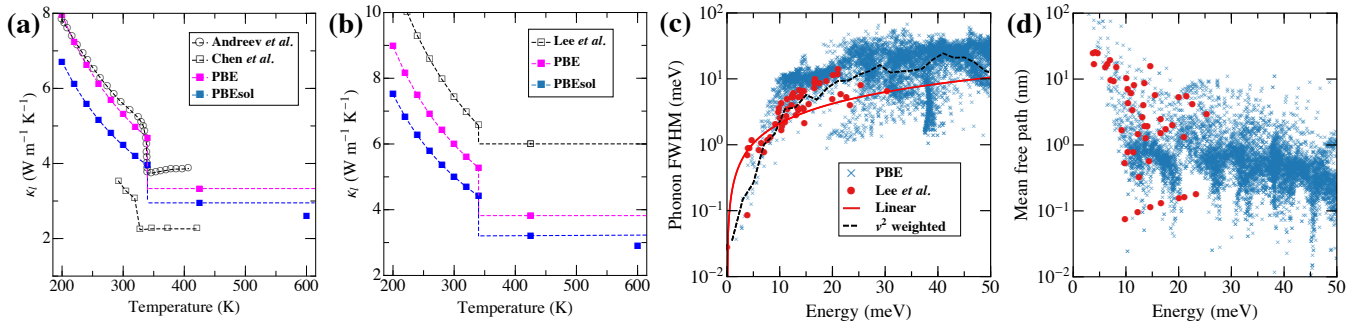


FIG. 2. (a) Computed lattice thermal conductivity of polycrystalline VO₂ using PBE and PBEsol exchange correlation functionals in comparison with experimental results reported by Andreev *et al.* [36] and Chen *et al.* [37]. (b) Computed lattice thermal conductivity of single-crystal VO₂ along rutile *c* axis in comparison with estimations by Lee *et al.* [10]. (c) and (d) Computed phonon mode full width at half maximum (FWHM) and mean free path (MFP) (blue crosses) using PBE exchange correlation functional in comparison with experimental measurements (red disks) at 425 K [10]. The solid red line denotes the linear relation between FWHM and phonon energy employed in Ref. [10]. The dashed black line denotes the phonon group velocity weighted FWHM averaged over phonon modes with similar energies.

the strong anisotropy of mode-dependent FWHM. Since the energy cumulative κ_l (see Fig. S7 [18]) shows that phonon modes with energies larger than 10 meV contribute about 70% of total κ_l , the κ_l of R-VO₂ estimated by linearly interpolated FWHMs in Ref. [10] is therefore overestimated. Note that the present predicted κ_l of R-VO₂ is also potentially overestimated because (1) the renormalized TA1 modes have larger energies than experimental measurements, which commonly lead to larger κ_l because of reduced scattering rates and increased group velocity, and (2) high-order phonon-phonon interactions beyond three phonon processes are neglected in our calculation. As a consequence, a substantial change of κ_l across the MIT is expected, suggesting that WF law might not be violated as strongly as demonstrated in Ref. [10]. To illustrate the drop of κ_l across the MIT upon heating, comparisons of mode-resolved phonon lifetime, group velocity and mean free path between M- and R-VO₂ are shown in Fig. S8(a)-(c) [18]. The phonon lifetimes of M-VO₂ are overall significantly longer than those of R-VO₂ except those near the center of Brillouin zone. The phonon group velocities of both R- and M-VO₂ are fairly similar. As a result, M-VO₂ has overall larger MFPs than R-VO₂, which is in opposition to Ref. [10], therefore explaining the significant change of κ_l across the MIT.

In summary, we have applied a first-principles-based phonon renormalization scheme on top of compressive sensing lattice dynamics to model lattice dynamics and thermal transport properties of VO₂ from low (monoclinic insulating VO₂) to high (rutile metallic VO₂) temperatures across the metal-insulator transition temperature (MIT). Using the obtained temperature-dependent 2nd- and 3rd-order interatomic force constants, we successfully computed temperature-dependent phonon dispersions of rutile VO₂ and identified its intrinsic strong

anharmonicity associated with low-lying zone-center optical mode. We also computed entropy change due to lattice vibrations across the MIT, based on which we found the contribution from magnetic ordering might also be important. Finally, lattice thermal transport properties were investigated for both phases and a significant change of κ_l across the MIT is confirmed, suggesting that Wiedemann-Franz law might not be strongly violated in R-VO₂.

Acknowledgements We wish to thank Huihuo Zheng for fruitful discussions. This work was performed at the Center for Nanoscale Materials, a U.S. Department of Energy Office of Science User Facility, and supported by the U.S. Department of Energy, Office of Science, under Contract No. DE-AC02-06CH11357. This research used resources of the National Energy Research Scientific Computing Center, a DOE Office of Science User Facility supported by the Office of Science of the U.S. Department of Energy under Contract No. DE-AC02-05CH11231.

-
- [1] A. Pergament, G. Stefanovich, V. Malinenko, and A. Velichko, *Advances in Condensed Matter Physics* **2015**, 26 (2015).
 - [2] R. M. Wentzcovitch, W. W. Schulz, and P. B. Allen, *Phys. Rev. Lett.* **72**, 3389 (1994).
 - [3] C. J. Hearn, *Journal of Physics C: Solid State Physics* **5**, 1317 (1972).
 - [4] A. Zylbersztejn and N. F. Mott, *Phys. Rev. B* **11**, 4383 (1975).
 - [5] V. Eyert, *Annalen der Physik* **11**, 650 (2002).
 - [6] J. B. Goodenough, *Journal of Solid State Chemistry* **3**, 490 (1971).
 - [7] J. D. Budai, J. Hong, M. E. Manley, E. D. Specht, C. W. Li, J. Z. Tischler, D. L. Abernathy, A. H. Said, B. M. Leu, L. A. Boatner, R. J. McQueeney, and O. Delaire, *Nature* **515**, 535 (2014).

- [8] C. N. Berglund and H. J. Guggenheim, *Phys. Rev.* **185**, 1022 (1969).
- [9] O. Hellman, P. Steneteg, I. A. Abrikosov, and S. I. Simak, *Phys. Rev. B* **87**, 104111 (2013).
- [10] S. Lee, K. Hippalgaonkar, F. Yang, J. Hong, C. Ko, J. Suh, K. Liu, K. Wang, J. J. Urban, X. Zhang, C. Dames, S. A. Hartnoll, O. Delaire, and J. Wu, *Science* **355**, 371 (2017).
- [11] H. Zheng and L. K. Wagner, *Phys. Rev. Lett.* **114**, 176401 (2015).
- [12] H. Zheng, *First Principles Quantum Monte Carlo Study of Correlated Electronic Systems*, Ph.D. thesis, University of Illinois at Urbana-Champaign (2016).
- [13] F. Zhou, W. Nielson, Y. Xia, and V. Ozoliņš, *Phys. Rev. Lett.* **113**, 185501 (2014).
- [14] N. R. Werthamer, *Phys. Rev. B* **1**, 572 (1970).
- [15] P. Souvatzis, O. Eriksson, M. Katsnelson, and S. Rudin, *Computational Materials Science* **44**, 888 (2009).
- [16] I. Errea, M. Calandra, and F. Mauri, *Phys. Rev. B* **89**, 064302 (2014).
- [17] A. van Roekeghem, J. Carrete, and N. Mingo, *Phys. Rev. B* **94**, 020303 (2016).
- [18] “Supplementary materials: Contains details on the computational methods presented in this work. Further more, detailed descriptions of the computational parameters, crystal structures, convergence of lattice thermal conductivity, effects of different exchange correlation functionals and structure relaxation on phonon dispersions, and phonon lifetimes and mean free paths are presented.”
- [19] J. M. Ziman, *Electrons and Phonons: The Theory of Transport Phenomena in Solids* (Clarendon Press, 1960).
- [20] M. Omini and A. Sparavigna, *Physica B* **212**, 101 (1995).
- [21] M. Omini and A. Sparavigna, *Phys. Rev. B* **53**, 9064 (1996).
- [22] D. A. Broido, M. Malorny, G. Birner, N. Mingo, and D. A. Stewart, *Appl. Phys. Lett.* **91**, 231922 (2007).
- [23] W. Li, L. Lindsay, D. A. Broido, D. A. Stewart, and N. Mingo, *Phys. Rev. B* **86**, 174307 (2012).
- [24] G. Kresse and J. Hafner, *Phys. Rev. B* **47**, 558 (1993).
- [25] G. Kresse and J. Hafner, *Phys. Rev. B* **49**, 14251 (1994).
- [26] G. Kresse and J. Furthmüller, *Comput. Mater. Sci.* **6**, 15 (1996).
- [27] G. Kresse and J. Furthmüller, *Phys. Rev. B* **54**, 11169 (1996).
- [28] P. E. Blöchl, *Phys. Rev. B* **50**, 17953 (1994).
- [29] J. P. Perdew, K. Burke, and Y. Wang, *Phys. Rev. B* **54**, 16533 (1996).
- [30] P. Hohenberg and W. Kohn, *Phys. Rev.* **136**, B864 (1964).
- [31] J. P. Perdew, K. Burke, and M. Ernzerhof, *Phys. Rev. Lett.* **77**, 3865 (1996).
- [32] J. P. Perdew, A. Ruzsinszky, G. I. Csonka, O. A. Vydrov, G. E. Scuseria, L. A. Constantin, X. Zhou, and K. Burke, *Phys. Rev. Lett.* **100**, 136406 (2008).
- [33] M. Ropo, K. Kokko, and L. Vitos, *Phys. Rev. B* **77**, 195445 (2008).
- [34] S. Kim, K. Kim, C.-J. Kang, and B. I. Min, *Phys. Rev. B* **87**, 195106 (2013).
- [35] D. B. McWhan, M. Marezio, J. P. Remeika, and P. D. Dernier, *Phys. Rev. B* **10**, 490 (1974).
- [36] V. N. Andreev, F. Chudnovskii, A. Petrov, and E. Terukov, *Phys. stat. sol.* **a**, 153 (1978).
- [37] J. Chen, X. Liu, X. Yuan, Y. Zhang, Y. Gao, Y. Zhou, R. Liu, L. Chen, and N. Chen, *Chinese Science Bulletin* **57**, 3393 (2012).